Performance Trade-off and Joint Waveform Design for MIMO-OFDM DFRC Systems

Tianchen Liu, Liang Wu, *Senior Member, IEEE*, Bo An, Zaichen Zhang, *Senior Member, IEEE*, Jian Dang, *Senior Member, IEEE* and Jiangzhou Wang, *Fellow, IEEE*

arXiv:2401.02081v1 [cs.IT] 4 Jan 2024

***Abstract*—Dual-functional radar-communication (DFRC) has attracted considerable attention. This paper considers the frequency-selective multipath fading environment and proposes DFRC waveform design strategies based on multiple-input and multiple-output (MIMO) and orthogonal frequency division multiplexing (OFDM) techniques. In the proposed waveform design strategies, the Cramer-Rao bound (CRB) of the radar system, the inter-stream interference (ISI) and the achievable rate of the communication system, are respectively considered as the performance metrics. In this paper, we focus on the performance trade-off between the radar system and the communication system, and the optimization problems are formulated. In the ISI minimization based waveform design strategy, the optimization problem is convex and can be easily solved. In the achievable rate maximization based waveform design strategy, we propose a water-filling (WF) and sequential quadratic programming (SQP) based algorithm to derive the covariance matrix and the precoding matrix. Simulation results validate the proposed DFRC waveform designs and show that the achievable rate maximization based strategy has a better performance than the ISI minimization based strategy.**

***Index Terms*—Dual-functional radar-communication, multiple-input and multiple-output, orthogonal frequency division multiplexing, multipath fading.**

I. Introduction

Due to the shortage of radio spectrum, radar and communication systems are expected to use the same frequency band [1–3]. In addition, both the hardware architecture and the system composition of radar system and communication system are similar [4]. Therefore, the concept of joint radar and communication (JRC) has been proposed with the aim of miniaturization and commercialization. It is expected that JRC technology will promote huge potential applications. For example, recently, drones have been widely used in transportation and geographic explorations. However, drones with aggressive purposes pose a threat to social security [5][6]. Thus, drone surveillance radars are usually deployed. By employing JRC technology, drone surveillance radars not only have the advantage of quick deployment, but also interact with each other by establishing communication links to improve the target-detection accuracy. Moreover, to realize automatic driving, the transmission delay should be less than 10ms, and the position accuracy should be better than 1 centimeter [7]. JRC technology is expected to provide stable and precise sensing to guarantee the safety of autonomous driving, and the communication link is established at the same time to reduce the latency [8]. Furthermore, JRC technology can reduce the number of antennas, and alleviate the problem of electromagnetic interference or compatibility [9]. Therefore, JRC technology will play an important role in future mobile communication and radar detection systems.

The waveform design, which is one of the most challenging researches in the JRC system, is mainly classified into two categories. The first category is that the radar system and the communication system co-exist [10][11], where one system treats the other system as interference [12]. Therefore, multiplexing techniques including space division multiplexing (SDM) [13–15], time division multiplexing (TDM) [16–18], frequency division multiplexing (FDM) [19][20], and code division multiplexing (CDM) [21][22] have been applied to mitigate the interference in the co-existing system. However, in these multiplexing schemes, the co-existing waveform has a low utilization because the radar system and the communication system cannot employ the same resources, and two different kinds of waveforms are usually used respectively for radar and communication.

The second category is that the radar system and the communication system are co-designed, which aims to develop a single waveform that can perform radar detection and communication functions simultaneously [23], and this waveform is called dual-functional radar-communication (DFRC) waveform. Compared with the co-existing waveform, the DFRC waveform has a higher degree of integration, thus it is more attractive to both academia and industry [24].

The DFRC waveform design includes the radar-centric design, the communication-centric design, and the joint waveform design. The main idea of the radar-centric design is to employ linear frequency modulation (LFM) signal, which is a traditional radar probing signal, as the communication information carrier. For example, amplitude shift keying (ASK) and phase shift keying (PSK) can be combined with LFM to design the DFRC waveform in [25][26]. In the communication-centric design, the traditional communication waveform is mainly employed, and the detection estimation parameters can be extracted through the echo of the transmitted communication signal [27–30]. Joint waveform design is neither based on existing radar waveform nor communication waveform, but jointly considers the performance of the DFRC system and aims to achieve a performance trade-off between the communication and the radar detection [23], [30–33].

A great quantity of work has been devoted to the research

T. Liu, L. Wu, B. An, Z. Zhang and J. Dang are with National Mobile Communications Research Laboratory, Southeast University, Nanjing 210096, China (e-mail: {220210764, wuliang, anbo, zczhang, dangjian}@seu.edu.cn).

J. Wang is with School of Engineering, University of Kent, Canterbury, CT2 7NT United Kingdom (e-mail: j.z.wang@kent.ac.uk).

of the joint waveform design. In [23], mutual communication user interference (MUI) was employed as the communication performance metric, and the mismatch degree between the actual beam pattern and the desired beam pattern was used to evaluate the radar performance. A low-complexity algorithm was proposed to balance the radar performance and the communication performance. In [31], the cross-correlation of the beam strength at different angles was involved as a new radar performance metric and the precoding matrices of the radar system and the communication system were optimized to achieve the performance trade-off. *Wang et al.* in [32] employed the system model and the performance matrix of [23], and used a reconfigurable intelligence surface (RIS) to achieve an additional degree of freedom (DoF). The Cramer-Rao bound (CRB) of the radar system was employed in [33], and a higher beam directivity was achieved. In [34] and [35], the sidelobe level of the transmit beam pattern was minimized, and the peak-to-average power ratio (PAPR) of the transmit signal was used as a constraint to guarantee the power amplification efficiency of the high power amplifiers (HPAs).

All the above works adopted the single-carrier modulation, and the flat fading channel model was used. However, the frequency-selective multipath fading channel is more reasonable in the high-rate transmission. Orthogonal frequency division multiplexing (OFDM) [36][37] is one of the key technologies in the fifth generation (5G) mobile communication for its robustness to the multipath fading. Besides, it has been proven to be valid for the radar detection in [28]. *Xu et al.* in [38] presented a complete processing strategy for the measurement of range, velocity, and angle based on OFDM signals. Meanwhile, a trade-off scheme that employed dedicated subcarriers to balance the radar performance and the communication performance was also proposed. However, different subcarriers in [38] used the same precoding matrix, which led to a performance degradation in the DFRC system. The beam strength radiated towards the detection target is usually greater than that towards the communication user. Therefore, a subcarrier power allocation scheme was proposed in [39] to satisfy the different power requirements of the radar system and the communication system. *Hu et al.* in [40] extended the work of [23] and the PAPR of the designed OFDM waveform was optimized to achieve a better communication performance.

In this paper, we consider a single communication user MIMO system in the frequency-selective multipath fading environment. The DFRC base station (BS) utilizes a single waveform to realize the downlink communication and the target detection simultaneously. Because the MUI minimization strategy used in [23] cannot be directly used in the frequency-selective multipath fading environment, we propose an OFDM based waveform design strategy, which can effectively combat the multipath fading, to minimize the inter-stream interference (ISI) of the communication system and the CRB of the radar system. Furthermore, the achievable rate maximization based waveform design strategy and the joint water-filling and sequential quadratic programming (WF-SQP) algorithm are proposed to further improve the communication performance through the cooperation of different antennas.

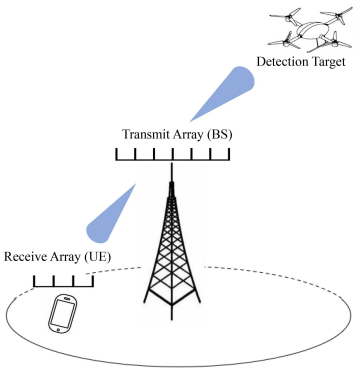

Fig. 1: Dual-functional radar-communication system.

The main contributions of this paper are summarized as follows:

1. We focus on the performance trade-off between the communication system and the radar system, and propose two OFDM based DFRC waveform design strategies to combat the frequency-selective multipath fading. In the first proposed DFRC waveform design strategy, we minimize the ISI of the communication system and the CRB of the radar system. The algorithms for designing the transmit covariance matrix and the precoding matrix design algorithms are proposed.

2. Different from the first DFRC waveform design strategy, the achievable rate of the communication system is employed in the second DFRC waveform design strategy. The performance trade-off is also considered. To derive the optimal transmit covariance matrix, a joint water-filling and SQP algorithm is proposed. Furthermore, the precoding matrix is derived analytically.

3. Simulation results are provided and analyzed in detail. Simulation results show that the proposed DFRC waveform design strategies can achieve satisfied communication and radar performances. The second proposed DFRC waveform design strategy achieves better radar and communication performances than the first one.

The rest of this paper is organized as follows. Section II presents the MIMO-OFDM based system model. In Section III, we propose the first OFDM based DFRC waveform design strategy with the aim of minimizing the ISI of the communication and the CRB of the radar. In Section IV, we maximize the achievable rate of the communication system, and propose the second waveform design strategy. Simulation results are provided in Section V. Finally, the conclusion is drawn in Section VI.

II. System model

Consider a MIMO-OFDM DFRC system, the BS is equipped with N_T antennas, and a uniform linear array (ULA) is employed. As shown in Fig. 1, the BS transmits signals for the target detection and the downlink communication at the same time. It is assumed that the number of the antennas equipped at the communication user equipment (UE) is N_R, and $N_R < N_T$.

The transmit signal vector $\boldsymbol{g}(n)$ is expressed as

$$\boldsymbol{g}(n) = [g_1(n), g_2(n), \cdots, g_{N_T}(n)]^T, n = 1, 2, \ldots, N + N_{CP} - 1, \tag{1}$$

where N is the size of inverse discrete Fourier transform (IDFT), N_{CP} is the length of the OFDM cyclic prefix, and $g_i(n)$ is the time-domain OFDM signal (including cyclic prefix) transmitted through the ith antenna. The transmit signal, $g_i(n)$ is given by

$$\begin{aligned}&[g_i(0), g_i(1), \cdots, g_i(N_{CP}-1), g_i(N_{CP}), \cdots, g_i(N+N_{CP}-1)]^T \\ &= [x_i(N-N_{CP}), \cdots, x_i(N-1), x_i(0), \cdots, x_i(N-1)], \\ &\qquad n = 1, 2, \ldots, N + N_{CP} - 1,\end{aligned} \tag{2}$$

where

$$x_i(n) = \frac{1}{N}\sum_{k=0}^{N-1} X_i(k) e^{j\frac{2\pi}{N}nk}, \tag{3}$$

and $X_i(k)$ is the frequency-domain signal at the kth subcarrier of the ith antenna.

The frequency-domain signal vector $\boldsymbol{X}(k)$ and the time-domain signal vector $\boldsymbol{x}(n)$ are expressed as

$$\boldsymbol{X}(k) = [X_1(k), X_2(k), \cdots, X_{N_T}(k)]^T, k = 0, 1, \ldots, N-1, \tag{4a}$$

$$\boldsymbol{x}(n) = [x_1(n), x_2(n), \cdots, x_{N_T}(n)]^T, n = 0, 1, \ldots, N-1. \tag{4b}$$

$$\boldsymbol{X}(k) = \boldsymbol{W}(k)\boldsymbol{S}(k), \tag{4c}$$

where $\boldsymbol{W}(k) \in \mathbb{C}^{N_T \times N_R}$ is the precoding matrix, and $\boldsymbol{S}(k) \in \mathbb{C}^{N_R}$ is the information vector.

The time-domain covariance matrix of the transmit signal is expressed as

$$\boldsymbol{R} = E\{\boldsymbol{x}(n)\boldsymbol{x}^H(n)\} \tag{5a}$$

$$\boldsymbol{R}(i,s) = \frac{1}{N^2} E\left\{\sum_{k_1}^{N-1}\sum_{k_2}^{N-1} X_i(k_1) X_s^*(k_2) e^{j\frac{2\pi}{N}n(k_1-k_2)}\right\}, \tag{5b}$$

where $E\{\cdot\}$ denotes the expectation of a random variable, $(\cdot)^H$ is the conjugate transpose operator, $(\cdot)^*$ is the conjugate operator and $\boldsymbol{R}(i,s)$ is the (i,s)th entry of $\boldsymbol{R}$. It is supposed that each antenna employs all the subcarriers, and $E\{\boldsymbol{X}_i(k_1)\boldsymbol{X}_s^*(k_2)\} = 0$ holds when $k_1 \neq k_2$. Therefore, Eq. (5a) can be rewritten as

$$\begin{aligned}\boldsymbol{R} &= \frac{1}{N^2} E\left\{\sum_{k=0}^{N-1} \boldsymbol{W}(k)\boldsymbol{S}(k)\boldsymbol{S}^H(k)\boldsymbol{W}^H(k)\right\} \\ &= \frac{1}{N^2}\sum_{k=0}^{N-1} \boldsymbol{W}(k)\boldsymbol{P}_S(k)\boldsymbol{W}^H(k),\end{aligned} \tag{6}$$

where $\boldsymbol{P}_S(k) = \mathrm{diag}\left\{p_{S_1(k)}, \cdots, p_{S_{N_R}(k)}\right\}$, $p_{S_i(k)}$ is the power of ith information stream at the kth subcarrier, and $\mathrm{diag}\{\cdot\}$ is the diagonal operator. The frequency-domain covariance matrix of the transmit signal at the kth subcarrier is defined as $\boldsymbol{R}_f(k) \in \mathbb{C}^{N_T \times N_T}$, and it is given by

$$\boldsymbol{R}_f(k) = E\{\boldsymbol{X}(k)\boldsymbol{X}^*(k)\} = \boldsymbol{W}(k)\boldsymbol{P}_S(k)\boldsymbol{W}^H(k). \tag{7}$$

The relationship between the frequency-domain and the time-domain covariance matrices can be expressed as

$$\frac{1}{N^2}\sum_{k=0}^{N-1} \boldsymbol{R}_f(k) = \boldsymbol{R}. \tag{8}$$

A. MIMO-OFDM Communication Model

The frequency-selective multipath fading channel model is employed, and the channel impulse response from the ith transmit antenna to the sth receive antenna is $h_{s,i}(n)$. The received signal at the sth receive antenna is given by

$$y_s(n) = \sum_{i=1}^{N_T} h_{s,i}(n) \otimes x_i(n) + z_s(n), s = 1, 2, \ldots, N_R, \tag{9}$$

where $\otimes$ denotes the convolution operation, and $z_s(n)$ is the noise component. In the frequency-domain, the received signal vector at the kth subcarrier can be expressed as

$$\begin{aligned}\boldsymbol{Y}(k) &= \boldsymbol{H}(k)\boldsymbol{X}(k) + \boldsymbol{Z}(k) \\ &= \boldsymbol{H}(k)\boldsymbol{W}(k)\boldsymbol{S}(k) + \boldsymbol{Z}(k), k = 0, 1, \ldots, N-1,\end{aligned} \tag{10}$$

where $\boldsymbol{H}(k) \in \mathbb{C}^{N_R \times N_T}$ is the frequency-domain channel matrix corresponding to the kth subcarrier, $\boldsymbol{Z}(k) \in \mathbb{C}^{N_R}$ is the frequency-domain Guassian noise vector with covariance matrix $\sigma_{\boldsymbol{Z}}^2 \boldsymbol{I}_{N_R}$, and $\boldsymbol{I}_{N_R}$ is an identical matrix with rank N_R.

The vector $\boldsymbol{Y}(k)$ can be rewritten as [23]

$$\boldsymbol{Y}(k) = \boldsymbol{S}(k) + \underbrace{\boldsymbol{H}(k)\boldsymbol{W}(k)\boldsymbol{S}(k) - \boldsymbol{S}(k)}_{\text{ISI}} + \boldsymbol{Z}(k). \tag{11}$$

The total power of ISI is

$$P_{\text{ISI}} = \sum_{k=0}^{N-1} \|\boldsymbol{H}(k)\boldsymbol{W}(k)\boldsymbol{S}(k) - \boldsymbol{S}(k)\|^2. \tag{12}$$

Therefore, when the ISI minimization principle is employed, the achievable rate of the system is given by

$$C_s = \sum_{k=0}^{N-1}\sum_{i=1}^{N_R} \frac{\Delta f}{B}\log_2\left(1 + \frac{E\{\|\boldsymbol{S}_i(k)\|^2\}}{E\{\|\boldsymbol{H}_i(k)\boldsymbol{W}(k)\boldsymbol{S}(k) - \boldsymbol{S}_i(k)\|^2\} + \sigma_{\boldsymbol{Z}}^2}\right), \tag{13}$$

where Δf is the subcarrier spacing, B is the bandwidth of the OFDM system, $\boldsymbol{S}_i(k)$ is the ith entry of $\boldsymbol{S}(k)$, and $\boldsymbol{H}_i(k)$ is the ith row of $\boldsymbol{H}(k)$. Note that the effect of the cyclic prefix to the data rate is ignored.

In the considered single user MIMO communication, the received signals of all antennas can be processed jointly. Therefore, the achievable rate in Eq. (13) can be increased. The maximum achievable rate of the considered single user MIMO communication system is given by [41]

$$C_t = \max\left\{\sum_{k=0}^{N-1} \frac{\Delta f}{B}\log_2\left(\det\left(\boldsymbol{I}_{N_R} + \frac{\boldsymbol{H}(k)\boldsymbol{R}_f(k)\boldsymbol{H}^H(k)}{\sigma_{\boldsymbol{Z}}^2}\right)\right)\right\}, \tag{14}$$

where $\det(\cdot)$ denotes the determinant of a matrix.

Although we focus on the single user communication scenario in this paper, the system model and the following proposed scheme can still be applied in the multiuser scenario, and time division multiple access (TDMA) technique can be used.

B. MIMO Radar Model

It is assumed that the detection target is a point target, and the echo signal received at the DFRC BS is given by

$$\begin{aligned}\boldsymbol{y}_r(n) &= \zeta \boldsymbol{a}(\theta)\boldsymbol{a}^H(\theta)\boldsymbol{x}(n) + \boldsymbol{z}_r(n) \\ &= \zeta \boldsymbol{A}(\theta)\boldsymbol{x}(n) + \boldsymbol{z}_r(n),\end{aligned} \tag{15}$$

where ζ is the reflection coefficient and contains the information of the radar cross section (RCS) of the target, $\boldsymbol{z}_r(n)$ is the Guassian noise vector, $\boldsymbol{A}(\theta) = \boldsymbol{a}(\theta)\boldsymbol{a}(\theta)^H$, θ is the angle of arrival of the target, and the steering vector $\boldsymbol{a}(\theta)$ is given by [33]

$$\begin{aligned}\boldsymbol{a}(\theta) =&[e^{-j2\pi\frac{(N_T-1)}{2}\Delta\sin\theta}, e^{-j2\pi\frac{(N_T-3)}{2}\Delta\sin\theta}, \\ &\cdots, e^{j2\pi\frac{(N_T-1)}{2}\Delta\sin\theta}]^T \in \mathbb{C}^{N_t\times 1},\end{aligned} \tag{16}$$

where the center of the ULA antennas is chosen as the reference point, and Δ is the normalized antenna spacing.

The CRB of θ can be derived as [42]

$$\mathrm{CRB}(\theta) = \frac{1}{2\mathrm{SNR}}\cdot \frac{\mathrm{tr}\left(\boldsymbol{A}^{\mathrm{H}}(\theta)\boldsymbol{A}(\theta)\boldsymbol{R}\right)}{\left(\left(\mathrm{tr}\left(\dot{\boldsymbol{A}}^{\mathrm{H}}(\theta)\dot{\boldsymbol{A}}(\theta)\boldsymbol{R}\right)\mathrm{tr}\left(\boldsymbol{A}^{\mathrm{H}}(\theta)\boldsymbol{A}(\theta)\boldsymbol{R}\right)\right) - \left|\mathrm{tr}\left(\dot{\boldsymbol{A}}^{\mathrm{H}}(\theta)\boldsymbol{A}(\theta)\boldsymbol{R}\right)\right|^2\right)}, \tag{17}$$

where $\dot{\boldsymbol{A}}(\theta) = \frac{\partial \boldsymbol{A}(\theta)}{\partial\theta}$, and $\mathrm{tr}(\cdot)$ is the operator of matrix trace. Substituding $\boldsymbol{A}(\theta) = \boldsymbol{a}(\theta)\boldsymbol{a}(\theta)^H$ into Eq. (17), the CRB of θ can be rewritten as

$$\mathrm{CRB}(\theta) = \frac{1}{2\mathrm{SNR}\|\dot{\boldsymbol{a}}(\theta)\|^2\boldsymbol{a}(\theta)^{\mathrm{H}}\boldsymbol{R}\boldsymbol{a}(\theta)}. \tag{18}$$

According to Eq. (18), the CRB of θ relies on the covariance matrix $\boldsymbol{R}$.

III. Joint waveform design based on CRB and ISI minimization

In this section, we first design the time-domain covariance matrix to minimize the CRB of θ. After that, an optimization problem of minimizing the interference among different information streams for a given time-domain covariance matrix is formulated, and the frequency-domain covariance matrix and the corresponding precoding matrix are designed. Besides, we propose the joint waveform design strategy based on the CRB and ISI minimization to achieve the performance trade-off.

A. Radar-only problem formulation

It is assumed that the detection target is located at the angle of θ. To minimize the CRB under the power constraint, the optimization problem can be formulated as follows

$$\mathrm{OP1}: \quad \arg\min_{\boldsymbol{R}} \frac{1}{2\mathrm{SNR}\|\dot{\boldsymbol{a}}(\theta)\|^2\boldsymbol{a}(\theta)^{\mathrm{H}}\boldsymbol{R}\boldsymbol{a}(\theta)} \tag{19a}$$

$$\text{s.t.} \quad \mathrm{tr}(\boldsymbol{R}) = P_T, \tag{19b}$$

$$\boldsymbol{R} = \boldsymbol{R}^H, \tag{19c}$$

where P_T is the total transmit power. The optimization problem OP1 is convex [43] and can be solved by CVX tools. The optimal time-domain covariance matrix is denoted by $\boldsymbol{R}_d$.

B. Radar-strict problem formulation and the precoding matrix design

Based on $\boldsymbol{R}_d$, the problem of minimizing the interference among different information streams is given by

$$\mathrm{OP2}: \quad \arg\min_{\boldsymbol{W}(\mathrm{k})} \left(\sum_{k=0}^{N-1} E\{\|\boldsymbol{H}(k)\boldsymbol{W}(k)\boldsymbol{S}(k) - \boldsymbol{S}(k)\|^2\}\right) \tag{20a}$$

$$\text{s.t.} \quad \boldsymbol{W}(k)\boldsymbol{P}_S(k)\boldsymbol{W}^H(k) = \boldsymbol{R}_f(k), \tag{20b}$$

$$\frac{1}{N^2}\sum_{k=1}^{N}\boldsymbol{R}_f(k) = \boldsymbol{R}_d. \tag{20c}$$

It is assumed that $E\left\{\boldsymbol{S}(k)\boldsymbol{S}^H(k)\right\} = E_s\boldsymbol{I}_{N_R}, k = 0,1,\ldots,N-1$. Therefore, problem OP2 is equivalent to

$$\mathrm{OP3}: \quad \arg\min_{\boldsymbol{W}(k)} \left(\sum_{k=0}^{N-1} \|\boldsymbol{H}(k)\boldsymbol{W}(k) - \boldsymbol{I}_{N_R}\|^2\right) \tag{21a}$$

$$\text{s.t.} \quad E_S\cdot\boldsymbol{W}(k)\boldsymbol{W}^H(k) = \boldsymbol{R}_f(k), \tag{21b}$$

$$\frac{1}{N^2}\sum_{k=1}^{N}\boldsymbol{R}_f(k) = \boldsymbol{R}_d. \tag{21c}$$

The above optimization problem is NP-hard and cannot be solved easily [43]. Therefore, the suboptimal frequency-domain covariance matrix $\boldsymbol{R}_f(k)$ and the frequency domain precoding matrix $\boldsymbol{W}(k)$ are derived as follows.

1) *The derivation of* $\boldsymbol{R}_f(k)$: according to Eq. (8), define

$$\boldsymbol{R}_f(k) = \alpha_k N^2\boldsymbol{R}_d, \tag{22}$$

where $\sum_{k=0}^{N-1}\alpha_k = 1$, and $\alpha_k \geq 0$. Besides, if $\boldsymbol{H}(k)\boldsymbol{W}(k) = \boldsymbol{I}_{N_R}$, it has

$$\left\|\boldsymbol{H}(k)\boldsymbol{W}(k)\boldsymbol{W}^H(k)\boldsymbol{H}^H(k) - \boldsymbol{I}_{N_R}\right\| = \left\|\boldsymbol{H}(k)\boldsymbol{W}(k) - \boldsymbol{I}_{N_R}\right\|, \tag{23}$$

and the optimization problem OP3 can be relaxed into

$$\mathrm{OP4}: \quad \arg\min_{\boldsymbol{\alpha}} \left(\sum_{k=0}^{N-1}\left\|\frac{\alpha_k N^2}{E_S}\boldsymbol{H}(k)\boldsymbol{R}_d\boldsymbol{H}^H(k) - \boldsymbol{I}_{N_R}\right\|^2\right) \tag{24a}$$

$$\text{s.t.} \sum_{k=0}^{N-1}\alpha_k = 1, \tag{24b}$$

$$\alpha_k \geq 0, k = 0,1,\ldots,N-1. \tag{24c}$$

The optimization problem OP4 is convex [43] and can be solved by CVX tools. The suboptimal frequency-domain covariance matrix $\boldsymbol{R}_f(k)$ can be obtained according to Eq. (22) and the derived optimal $\boldsymbol{\alpha}$.

2) *The derivation of* $\boldsymbol{W}(k)$: define $\boldsymbol{\Gamma}(k) = \boldsymbol{R}_f(k)/E_S$. By applying Cholesky decomposition, we can obtain

$$\boldsymbol{T}(k)\boldsymbol{T}^H(k) = \boldsymbol{\Gamma}(k), \tag{25}$$

where $\boldsymbol{T}(k)$ is an invertible lower triangular matrix. Therefore, constraint (21b) can be rewritten as

$$\boldsymbol{T}^{-1}(k)\boldsymbol{W}(k)\boldsymbol{W}^H(k)\boldsymbol{T}^{-H}(k) = \boldsymbol{I}_{N_T}. \tag{26}$$

Defining $\widetilde{\boldsymbol{W}}(k)=\boldsymbol{T}^{-1}(k)\boldsymbol{W}(k)$, the optimization problem OP3 can be split into N subproblems, and the kth subproblem is given by

$$\text{OP5}: \quad \arg\min_{\widetilde{\boldsymbol{W}}} \left(\left\| \boldsymbol{H}(k)\boldsymbol{T}(k)\widetilde{\boldsymbol{W}}(k)-\boldsymbol{I}_{N_R} \right\|^2 \right) \tag{27a}$$

$$\text{s.t.} \quad \widetilde{\boldsymbol{W}}(k)\widetilde{\boldsymbol{W}}^{H}(k)=\boldsymbol{I}_{N_T}. \tag{27b}$$

The optimization problem OP5 is an Orthogonal Procrustes problem (OPP) problem, and it has a globally optimal solution, which is given by [44]

$$\widetilde{\boldsymbol{W}}(k)=\widetilde{\boldsymbol{U}}(k)\boldsymbol{I}_{N_T\times N_R}\widetilde{\boldsymbol{V}}^{H}(k), \tag{28}$$

where $\boldsymbol{I}_{N_T\times N_R}$ is a diagonal matrix and each diagonal element is equal to one, $\widetilde{\boldsymbol{U}}(k)\boldsymbol{\Sigma}(k)\widetilde{\boldsymbol{V}}^{H}(k)$ is the Singular Value Decomposition (SVD) of $\boldsymbol{T}^{H}(k)\boldsymbol{H}^{H}(k)$. Finally, the suboptimal precoding matrix can be derived as

$$\boldsymbol{W}(k)=\boldsymbol{T}(k)\widetilde{\boldsymbol{U}}(k)\boldsymbol{I}_{N_T\times N_R}\widetilde{\boldsymbol{V}}^{H}(k). \tag{29}$$

C. DFRC performance trade-off problem formulation and precoding matrix design

Note that in the optimization problem OP2, the transmit covariance matrix strictly conforms to the optimal result of the Radar-only problem in Section 3.1. Because of this, the communication performance is greatly degraded, and the interference among different information streams at the receiver is serious. Therefore, we consider a trade-off problem, and extend the traditional work in [23] to the frequency-selective multipath channel, where communication performance (ISI among different data streams) and the radar performance (CRB of radar detection) are balanced.

The suboptimal precoding matrix derived in Section 3.2 is denoted by $\boldsymbol{W}_d(k)$, and the trade-off problem is formulated as [23]

$$\text{OP6}: \quad \arg\min_{\boldsymbol{W}} \sum_{\mathrm{k=0}}^{\mathrm{N-1}} \rho_1\|\boldsymbol{H}(k)\boldsymbol{W}(k)\boldsymbol{S}(k)-\boldsymbol{S}(k)\|^2 + (1-\rho_1)\|\boldsymbol{W}(k)-\boldsymbol{W}_d(k)\|^2 \tag{30a}$$

$$\text{s.t.} \quad \frac{E_S}{N^2}\mathrm{tr}\left(\sum_{k=0}^{N-1}\boldsymbol{W}(k)\boldsymbol{W}^{H}(k)\right)\le P_T, \tag{30b}$$

where $\rho_1\in[0,1]$ is a given weighting factor that balances the radar performance and the communication performance. The optimization problem OP6 can be relaxed into N simplified subproblems, and the kth subproblem is expressed as

$$\text{OP7}: \quad \arg\min_{\boldsymbol{W}(k)} \rho_1\|\boldsymbol{H}(k)\boldsymbol{W}(k)-\boldsymbol{I}_{N_R}\|^2 + (1-\rho_1)\|\boldsymbol{W}(k)-\boldsymbol{W}_d(k)\|^2 \tag{31a}$$

$$\text{s.t.} \quad \mathrm{tr}\left(\boldsymbol{W}(k)\boldsymbol{W}^{H}(k)\right)\le \mathrm{tr}\left(\boldsymbol{W}_d(k)\boldsymbol{W}_d^{H}(k)\right). \tag{31b}$$

The above optimization problem is convex and the optimal frequency-domain precoding matrix $\boldsymbol{W}(k)$ can be obtained.

IV. Joint waveform design based on CRB minimization and achievable rate maximization

In [23], [30–33] and [40], different receive antennas belong to different communication users, and each user is equipped with one antenna. In this paper, a single communication user MIMO scenario is considered, and all the receive antennas belong to the same user. However, there is no related integrated signal design method in the considered scenario. In this section, we propose a joint waveform design strategy based on the CRB minimization and achievable rate maximization.

A. Communication-only problem formulation

The maximum achievable rate of the communication system is given in Eq. (14). Under the power constraint, the communication-only optimization problem can be formulated as

$$\text{OP8}: \arg\max_{\boldsymbol{W}(k),\boldsymbol{P}_S(k)} \left\{ \sum_{k=0}^{N-1}\frac{\Delta f}{B} \cdot \log_2\left(\det\left(\boldsymbol{I}+\frac{\boldsymbol{H}(k)\boldsymbol{W}(k)\boldsymbol{P}_S(k)\boldsymbol{W}^{H}(k)\boldsymbol{H}^{H}(k)}{\sigma_{\boldsymbol{Z}}^2}\right)\right)\right\} \tag{32a}$$

$$\text{s.t.} \quad \frac{1}{N^2}\sum_{k=0}^{N-1}\mathrm{tr}(\boldsymbol{W}(k)\boldsymbol{P}_S(k)\boldsymbol{W}^{H}(k))=P_T. \tag{32b}$$

The above optimization problem OP8 can be solved through the traditional water-filling algorithm, and according to Eq. (6), the optimal frequency-domain covariance matrix is

$$\boldsymbol{R}_{f,com}(k)=\boldsymbol{W}_{com}(k)\boldsymbol{P}_{S,com}(k)\boldsymbol{W}_{com}^{H}(k), \tag{33}$$

where $\boldsymbol{W}_{com}(k)$ is the optimal precoding matrix and $\boldsymbol{P}_{S,com}(k)$ is the corresponding power allocation matrix. According to the traditional water-filling algorithm, $\boldsymbol{W}_{com}(k)$ is given by

$$\boldsymbol{W}_{com}(k)=\boldsymbol{V}_{com}(k), \tag{34}$$

where $\boldsymbol{U}_{com}(k)\boldsymbol{\Sigma}_{com}(k)\boldsymbol{V}_{com}^{H}(k)$ is the SVD of $\boldsymbol{H}(k)$.

B. Covariance matrix design for DFRC performance trade-off

In this subsection, we balance the communication performance (achievable rate) and the radar performance (CRB of radar detection), and propose an algorithm based on the water-filling algorithm and sequential quadratic programming (SQP) method, which is referred to as the WF-SQP algorithm, to derive the covariance matrix of the transmit signal.

We divide the time-domain covariance matrix $\boldsymbol{R}$ into two parts to achieve the performance trade-off, that is,

$$\boldsymbol{R}=\boldsymbol{R}_1+\boldsymbol{R}_2, \tag{35}$$

where $\boldsymbol{R}_1$ and $\boldsymbol{R}_2$ are all nonnegative definite hermite matrix. The corresponding power are defined as

$$\begin{cases} P_1=\mathrm{tr}(\boldsymbol{R}_1) \\ P_2=\mathrm{tr}(\boldsymbol{R}_2) \\ P_T=P_1+P_2. \end{cases} \tag{36}$$

Define $\rho_2 = P_1/P_T$ as the trade-off factor in this waveform design strategy. Note that the total power P_T is divided into two parts (P_1 and P_2) for optimization, and both parts are employed for the radar system and the communication system. The derivation of the frequency domain covariance matrix is as follows.

Step 1: Substitute P_1 for P_T in Eq. (32b), and the corresponding optimal frequency-domain covariance matrix $\boldsymbol{R}_{f,1}(k)$ can be derived based on the water-filling algorithm.

Step 2: Consider the performance trade-off, and set $\boldsymbol{R}_2 = (1-\rho_2)\boldsymbol{R}_d$, According to Eq. (22), the corresponding frequency-domain covariance matrix at each subcarrier is set as $\boldsymbol{R}_{f,2}(k) = \omega_k N^2 \boldsymbol{R}_2$, where $\omega_k \geq 0$ is the weighting coefficient for each subcarrier and $\sum_{k=0}^{N-1} \omega_k = 1$.

Step 3: Based on the above two steps, the optimization problem to maximize the achievable rate is given by

$$\begin{aligned} \text{OP9}: \quad & \arg\max_{\boldsymbol{\omega}} \sum_{k=0}^{N-1} \frac{\Delta f}{B} \\ & \cdot \log_2 \left(\det \left(\boldsymbol{I} + \frac{\boldsymbol{H}(k) \left(\boldsymbol{R}_{f,1}(k) + \omega_k N^2 \boldsymbol{R}_2 \right) \boldsymbol{H}^H(k)}{\sigma_{\boldsymbol{Z}}^2} \right) \right) \quad (37a) \\ & \text{s.t.} \quad \sum_{k=0}^{N-1} \omega_k = 1, \quad (37b) \\ & \omega_k \geq 0, k = 0, 1, 2, \ldots, N-1, \quad (37c) \end{aligned}$$

where $\boldsymbol{\omega} = [\omega_0, \omega_1, \ldots, \omega_{N-1}]^T$, and the optimal $\boldsymbol{\omega}$ can be obtained by the following SQP method.

Define the optimization objective function as

$$\begin{aligned} f(\boldsymbol{\omega}) = & - \sum_{k=0}^{N-1} \frac{\Delta f}{B} \\ & \cdot \log_2 \left(\det \left(\boldsymbol{I} + \frac{\boldsymbol{H}(k) \left(\boldsymbol{R}_{f,1}(k) + \omega_k N^2 \boldsymbol{R}_2 \right) \boldsymbol{H}^H(k)}{\sigma_{\boldsymbol{Z}}^2} \right) \right), \quad (38) \end{aligned}$$

and the constraints are

$$\begin{aligned} & v(\boldsymbol{\omega}) = \sum_{k=0}^{N-1} \omega_k - 1 = \mathbf{1}\boldsymbol{\omega} - 1, \quad (39a) \\ & g_k(\boldsymbol{\omega}) = -\omega_k = -\boldsymbol{e}_k \boldsymbol{\omega}, k = 0, 1, \ldots, N-1, \quad (39b) \end{aligned}$$

where $\mathbf{1} = [1, 1, \cdots, 1]$, and $\boldsymbol{e}_k = [0, 0, \cdots, \underbrace{1}_{k\text{th}}, \cdots, 0]$ is the unit vector. The optimization problem OP9 can be rewritten by

$$\begin{aligned} \text{OP10}: \quad & \arg\min_{\boldsymbol{\omega}} f(\boldsymbol{\omega}) \quad (40a) \\ & \text{s.t.} \quad v(\boldsymbol{\omega}) = 0, \quad (40b) \\ & g_k(\boldsymbol{\omega}) \leq 0, k = 0, 1, \ldots, N-1. \quad (40c) \end{aligned}$$

The nonlinear function $f(\boldsymbol{\omega})$ can be transformed into quadratic functions at the iteration point $\boldsymbol{\omega}_{(m)}$ through Taylor expansion, and the objective function is given by

$$\begin{aligned} & \frac{1}{2}[\boldsymbol{\omega} - \boldsymbol{\omega}_{(m)}]^T \nabla^2 f(\boldsymbol{\omega}_{(m)}) [\boldsymbol{\omega} - \boldsymbol{\omega}_{(m)}] \\ & \quad + \nabla f(\boldsymbol{\omega}_{(m)})^T [\boldsymbol{\omega} - \boldsymbol{\omega}_{(m)}]. \quad (41) \end{aligned}$$

Define $\boldsymbol{\eta} = \boldsymbol{\omega} - \boldsymbol{\omega}_{(m)}$, and OP10 is equivalent to:

$$\begin{aligned} \text{OP11}: \quad & \arg\min_{\boldsymbol{\eta}} \frac{1}{2} \boldsymbol{\eta}^T \nabla^2 f(\boldsymbol{\omega}_{(m)}) \boldsymbol{\eta} + \nabla f(\boldsymbol{\omega}_{(m)})^T \boldsymbol{\eta} \quad (42a) \\ & \text{s.t.} \quad 1\boldsymbol{\eta} = 1 - 1\boldsymbol{\omega}_{(m)}, \quad (42b) \\ & -\boldsymbol{e}_k \boldsymbol{\eta} \leq \boldsymbol{e}_k \boldsymbol{\omega}_{(m)}, k = 0, 1, \ldots, N-1. \quad (42c) \end{aligned}$$

The optimization problem OP11 is a standard Quadratic Programming (QP) problem with respect to $\boldsymbol{\eta}$, and it can be solved by using Lagrange multiplier method. The iterative steps of the SQP algorithm are summarized in Algorithm I.

Algorithm I: Algorithm for solving OP9

Input: convergence precision ϵ, $\boldsymbol{H}$, $\boldsymbol{R}_{f,1}(k)$, $\boldsymbol{R}_2$, $\sigma_{\boldsymbol{Z}}^2$, N.
Output: $\boldsymbol{\omega}_{(m)}$.
1. Initialize $\boldsymbol{\omega}_{(0)} = \frac{1}{N}\mathbf{1}$, $\|\boldsymbol{\omega}_{(1)} - \boldsymbol{\omega}_{(0)}\| > \varepsilon$, $m = 0$.
while $\|\boldsymbol{\omega}_{(1)} - \boldsymbol{\omega}_{(0)}\| > \varepsilon$
2. Transform the original problem OP9 to a QP problem OP11 at the iteration point $\boldsymbol{\omega}_{(m)}$.
3. Compute $\nabla^2 f(\boldsymbol{\omega}_{(m)})$ through Davidon-Fletcher-Powell (DFP) algorithm or Broyden-Fletcher-Goldfarb-Shanno (BFGS) algorithm [45][46].
4. Solve the QP problem and obtain the optimal result $\boldsymbol{\eta}^*$.
5. Compute $\boldsymbol{\omega}_{(m+1)} = \boldsymbol{\omega}_{(m)} + \boldsymbol{\eta}^*$.
6. $m = m + 1$.
end while

After obtaining the optimal result $\boldsymbol{\omega}$, $\boldsymbol{R}_{f,2}(k)$ can be derived based on $\boldsymbol{R}_{f,2}(k) = \omega_k N^2 \boldsymbol{R}_2$, and the frequency-domain covariance matrix can be derived as $\boldsymbol{R}_f(k) = \boldsymbol{R}_{f,1}(k) + \boldsymbol{R}_{f,2}(k)$.

C. Precoding matrix design for the DFRC performance trade-off

For a given power P_1, we can obtain the optimal precoding matrix $\boldsymbol{W}_1(k)$ based on Eq. (34) and the corresponding power allocation matrix $\boldsymbol{P}_{S,1}(k)$ through water-filling algorithm. According to Eq. (33), $\boldsymbol{R}_{f,1}(k)$ should satisfy

$$\boldsymbol{R}_{f,1}(k) = \boldsymbol{W}_1(k) \boldsymbol{P}_{S,1}(k) \boldsymbol{W}_1^H(k), \quad (43)$$

where $\boldsymbol{P}_{S,1}(k) = \text{diag}\{p_{S_1,1}(k), \cdots p_{S_{N_R},1}(k)\}$, $p_{S_i,1}(k)$ is the power allocated to the ith information stream at the kth subcarrier according to the water-filling algorithm, and $\sum_{k=0}^{N-1} \text{tr}\left(\boldsymbol{P}_{S,1}(k)\right) = P_1$.

Similarly, $\boldsymbol{R}_{f,2}(k)$ should satisfy

$$\boldsymbol{R}_{f,2}(k) = \boldsymbol{W}_2(k) \boldsymbol{P}_{S,2}(k) \boldsymbol{W}_2^H(k). \quad (44)$$

Since $\frac{P_1}{P_2} = \frac{\rho_2}{1-\rho_2}$, we can set $\boldsymbol{P}_{S,2}(k)$ as

$$\boldsymbol{P}_{S,2}(k) = \frac{1-\rho_2}{\rho_2} \boldsymbol{P}_{S,1}(k). \quad (45)$$

Define $\boldsymbol{P}^{\circ}(k)=\left(\boldsymbol{P}_{S,1}(k)\right)^{1/2}$, substitute Eq. (45) into Eq. (44), and $\boldsymbol{R}_{f,2}(k)$ can be derived as

$$\boldsymbol{R}_{f,2}(k)=\frac{1-\rho_2}{\rho_2}\boldsymbol{W}_2(k)\boldsymbol{P}^{\circ}(k)\left(\boldsymbol{W}_2(k)\boldsymbol{P}^{\circ}(k)\right)^H. \quad (46)$$

The sizes of $\boldsymbol{R}_{f,2}(k)$, $\boldsymbol{W}_2(k)$, $\boldsymbol{P}^{\circ}(k)$ are $N_T\times N_T$, $N_T\times N_R$, and $N_R\times N_R$, respectively. Note that $N_R<N_T$ is assumed in this paper. Therefore, according to Eq. (46), we can derive the approximate solution of the precoding matrix $\boldsymbol{W}_2(k)$ as [47]

$$\boldsymbol{W}_2(k)=\boldsymbol{Q}(k)\left(\boldsymbol{D}(k)\right)^{1/2}\boldsymbol{I}_{N_T\times N_R}\left((\boldsymbol{P})^{\circ}(k)\right)^{-1}, \quad (47)$$

where $\boldsymbol{Q}(k)\boldsymbol{D}(k)\boldsymbol{Q}^{-1}(k)=\frac{\rho_2}{1-\rho_2}\boldsymbol{R}_{f,2}(k)$ is the eigenvalue decomposition of $\boldsymbol{R}_{f,2}(k)$.

Finally, the frequency-domain precoding matrix is designed as

$$\boldsymbol{W}(k)=\sqrt{\frac{1-\rho_2}{\rho_2}}\boldsymbol{W}_2(k)+\boldsymbol{W}_1(k), k=0,1,\ldots,N-1. \quad (48)$$

In summary, the waveform design strategy based on the WF-SQP algorithm is provided in Algorithm II.

Algorithm II: The waveform design strategy based on the CRB minimization and achievable rate maximization

Input: convergence precision ϵ, $\boldsymbol{H}$, N, P_T, θ, ρ_2.
Output: $\boldsymbol{W}(k), k=0,1,\ldots,N-1$.
1. Solve the Radar-only problem OP1 and obtain $\boldsymbol{R}_d$.
2. For a given ρ_2, calculate P_1 and solve the Communication -only problem OP8 under the power constraint P_1. Obtain the optimal $\boldsymbol{R}_{f,1}(k)$, $\boldsymbol{W}_1(k)$, and $\boldsymbol{P}_{S,1}(k)$ by using the water -filling algorithm.
3. Set $\boldsymbol{R}_2=(1-\rho_2)\boldsymbol{R}_d$. Based on $\boldsymbol{R}_2$ and $\boldsymbol{R}_{f,1}(k)$, solve the problem OP9 through SQP method and obtain $\boldsymbol{\omega}$.
4. Calculate $\boldsymbol{R}_{f,2}(k)$, according to $\boldsymbol{R}_{f,2}(k)=\omega_k N^2\boldsymbol{R}_2$.
5. Calculate the precoding matrix $\boldsymbol{W}_2(k)$ based on Eq. (47).
6. Derive the precoding matrix $\boldsymbol{W}(k)$ according to Eq. (48).

It is noteworthy that PAPR is one of the most important factors in both communication and radar systems, and traditional PAPR reduction strategies [48][49] can be employed in the proposed DFRC system to ensure the effectiveness of radar detection and communication service.

D. Complexity analysis

The idea of SQP algorithm is to solve quadratic programming problems through multiple iterations. In the Lagrange method employed in the proposed scheme, we need to solve a $(N+M)\times(N+M)$ linear equation system, where M is the number of constraints. The complexity of solving it using Gaussian elimination method is $O((N+M)^3)$. In this paper, it is assumed that $M=2$ and the number of convergency iterations of the SQP algorithm is K_{SQP} , and the complexity of the SQP algorithm is $O(K_{\mathrm{SQP}}(N+2)^3)$.

For the optimization problems considered in this paper, we can also employ other nonlinear optimization algorithms, such as the Interior Point Method (IPM). The complexity analysis of IPM is as follows:

In each iteration of IPM, solving the Newton equation dominates the time complexity. The complexity of solving the Newton equation is $O(MN^3+M^2N^2+M^3+N^3)$[50]. It is assumed the number of convergency iterations is K_{IPM}, and $M=2$. Therefore, the complexity of IPM is $O(K_{\mathrm{IPM}}(3N^3+4N^2))$.

Increasing the number of OFDM subcarriers N will mainly benefit the communication system, because it will enhance system anti-interference ability and improve the frequency efficiency. However, it should be noted that increasing the number of subcarriers can also increase the complexity and power consumption of the DFRC system, and may have a certain impact on transmission delay. Therefore, the number of subcarriers needs to be flexibly adjusted according to the actual scenario.

In this paper, the optimal point derived by IPM and SQP are consistent. Because SQP has a lower complexity, we employ the SQP algorithm in the proposed scheme.

V. Simulation results

In this section, we verify the proposed waveform design strategies through simulations. The total transmit power P_T is normalized to be 1, and each entry of the frequency-domain channel matrix $\boldsymbol{H}(k)$ is subject to standard complex Gaussian distribution. The DFRC BS is equipped with $N_T=20$ antennas. The number of receive antennas at the communication user is $N_R=10$. The data streams are modulated by quadrature phase shift keying (QPSK). The number of the OFDM subcarriers is $N=16$. The interested detection target is located at the angle of 0°. In the figures, the traditional scheme in [23] labelled with 'Traditional scheme' is provided as the benchmark scheme, the designs with the strict CRB minimization constraint (mentioned in Section III B) and the performance trade-off are labelled with 'Strict' and 'Trade-off', respectively, and we use 'ISI-min' (inter-stream interference minimization), and 'AR-max' (achievable rate maximization) to distinguish the proposed two strategies. Note that the precoding matrix design corresponding to 'AR-max' strategy in Eq. (47) is an approximate solution, thus the derived achievable rate using the proposed precoding design will be lower than the ideal optimal result of OP9, and these two cases are labelled as 'Actual' and 'Ideal', respectively.

The symbol error rates (SERs) of the proposed waveform design strategies are plotted in Fig. 2. Note that the frequency-selective multipath fading channel is considered in this paper, the scheme in [23] labelled by 'Traditional scheme' cannot be directly applied to achieve a satisfied result. It can be seen from Fig. 2 that the 'Strict' design suffers great communication performance loss under the strict equality constraint (20a)(20b), and the communication performance can be improved by introducing the trade-off factor. Fig. 2 also shows the performance of the proposed 'Trade-off' design strategy based on the CRB and ISI minimization, which is an extension of the work in [23] to the frequency-selective multipath fading environment. It can be also seen from Fig. 2 that the second proposed waveform design strategy based on the CRB minimization and the achievable rate maximization achieves the best SER performance.

Fig. 3 shows the achievable rate of the proposed waveform design strategies. It can be seen from Fig. 3 that the proposed

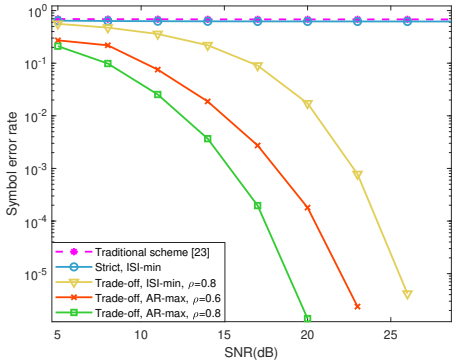

Fig. 2: Symbol error rate comparison of different strategies with different SNR.

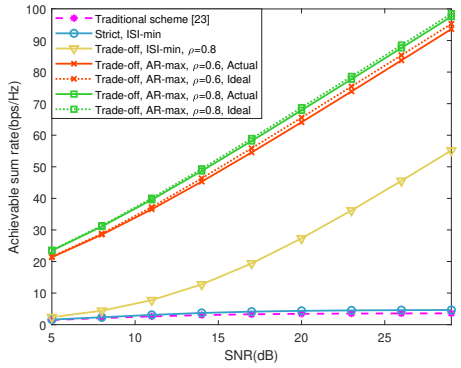

Fig. 3: Achievable rate comparison of different strategies with different SNR.

waveform design strategy based on the achievable rate maximization outperforms the strategy based on ISI minimization. Furthermore, it is noteworthy that by employing the proposed precoding matrix design in Eq. (48), the achievable rate only experiences a slight performance loss compared to the ideal optimal result of OP9.

The SER versus the trade-off factor is shown in Fig. 4, where SNR is 20 dB. It can be seen from Fig. 4 that the SERs of the proposed two waveform design strategies decrease

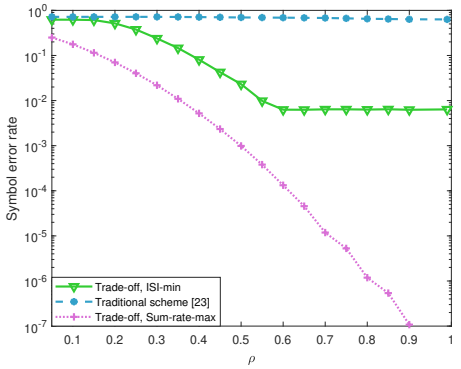

Fig. 4: Symbol error rate comparison of different strategies with different trade-off factors, SNR=20 dB.

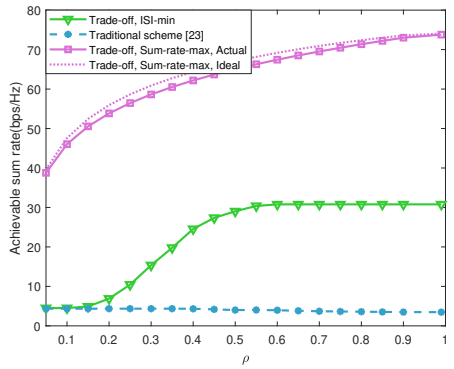

Fig. 5: Achievable rate comparison of different strategies with different trade-off factors, SNR=20 dB.

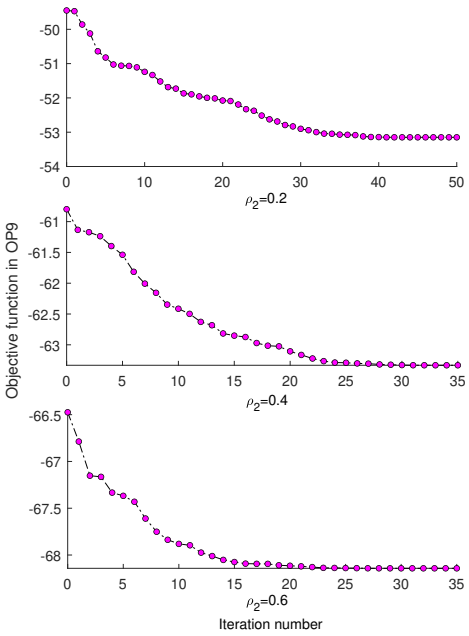

Fig. 6: Convergence performance verification of the proposed WF-SQP algorithm.

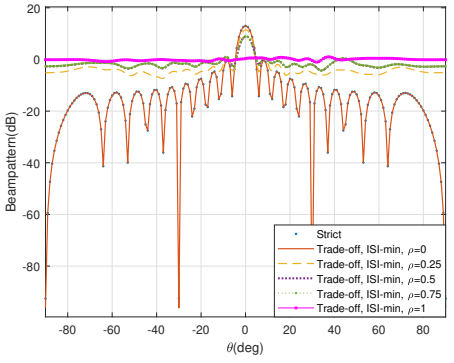

Fig. 7: Radar beam pattern obtained by the 'ISI-min' strategy with different trade-off factors.

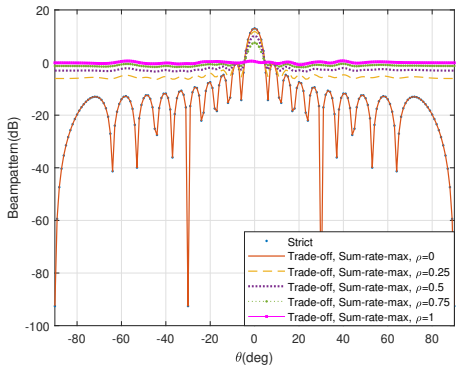

Fig. 8: Radar beam pattern obtained by the 'AR-max' strategy with different trade-off factors.

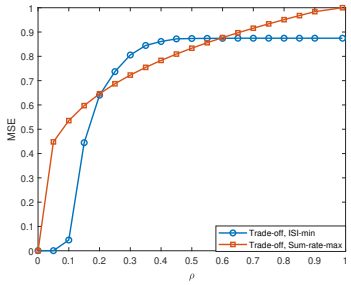

Fig. 9: NMSEs of radar beam pattern obtained by different strategies.

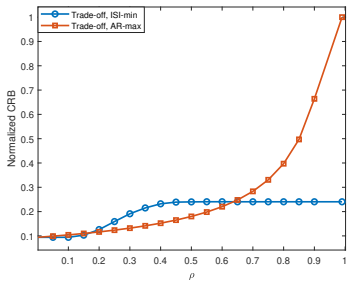

Fig. 10: Normalized CRBs obtained by different strategies.

with the increase of the trade-off factor. In the first waveform design strategy (ISI-min), when the trade-off factor is greater than 0.6, there is an error floor. That is because when the first term in Eq. (31a) is close to 0, there is a communication performance bound of this strategy. For the second waveform design strategy (AR-max), there is no error floor, which proves the superiority of the proposed 'AR-max' strategy.

Fig. 5 shows achievable rate versus the trade-off factor, and SNR is also equal to 20 dB. The achievable rates of the two waveform design strategies get improved with the increase of trade-off factor. Moreover, the communication performance of the 'AR-max' strategy continuously improves with the increase of trade-off factor, while the 'ISI-min' based strategy reaches its performance bound when the trade-off factor is greater than 0.6, which is similar to the results in Fig. 4. Meanwhile, the stability of the second proposed waveform design strategy (AR-max) is also verified in Fig. 5, and the gap between the actual result and the ideal optimal result in OP9 is very small.

It is noteworthy that the 'AR-max' strategy and 'ISI-min' strategy are fundamentally different. The aim of 'ISI-min' strategy is to minimize the interference among the signals of different receive antennas, and the signals of different receive antennas do not need to be jointly processed. The aim of the 'AR-max' strategy is to maximize the achievable sum rate, and the receiver jointly processes the signals of different receive antennas, which achieves better performance than the 'ISI-min' strategy. Therefore, the SER and achievable rate performances of the 'AR-max' strategy are better than those of the 'ISI-min' strategy.

Fig. 6 shows the variation of the objective function in OP9 with the iteration number of the WF-SQP algorithm. The convergence performance of different trade-off factors are compared in Fig. 6. The convergence precision ϵ is set to be 10^{-6}, and SNR is $20\,\mathrm{dB}$. It can be seen from Fig. 6 that for each trade-off factor, the objective function decreases with the increase of iteration number. Furthermore, the termination conditions are satisfied within 40 iterations. Therefore, the convergence performance of the proposed WF-SQP algorithm can achieve a good performance.

The resultant radar beampatterns obtained by the two proposed strategies with different trade-off factors are provided in Fig. 7 and Fig. 8, respectively. The 'Strict' beam pattern corresponds to the optimal result of OP1. It can be seen from Fig. 7 and Fig. 8 that when the trade-off factor equals 0, the proposed two performance trade-off waveform design strategies obtain the same beam pattern as the 'Strict' beam pattern. Meanwhile, with the increase of trade-off factor, the mismatch between the obtained beam pattern and the 'Strict' beam pattern begins to increase, because the radar performance is sacrificed to enhance the communication performance.

We employ the normalized mean square error (NMSE) to describe the beampattern mismatch. The NMSE is defined as

$$\mathrm{NMSE} = \frac{\int \|\mathrm{B_S}(\theta) - \mathrm{B_T}(\theta)\|^2 \mathrm{d}\theta}{\int \|\mathrm{B_S}(\theta)\|^2 \mathrm{d}\theta}, \tag{49}$$

where $B_S(\theta)$ is the 'Strict' beam pattern, and $B_T(\theta)$ is the beam pattern with 'Trade-off' strategy.

The beampattern NMSEs of different strategies with different trade-off factors are plotted in Fig. 9, and the normalized CRBs obtained by different strategies are provided in Fig. 10, which is consistent with Fig. 9. It can be observed that for trade-off factor within $[0.2, 0.6]$, the NMSE of the 'AR-max' strategy is lower than that of the 'ISI-min' strategy, which means a lower CRB for the target detection. From Fig. 4 and Fig. 5, when the trade-off factor is less than 0.2, the communication performance is not acceptable (with SER$\geq 10\%$); when the trade-off factor is greater than 0.6, the communication performance of the 'ISI-min' strategy keeps the same, which means the communication performance cannot be improved with the increase of the trade-off factor. Therefore, the trade-off factor works in the range of $[0.2, 0.6]$ for the 'ISI-min' strategy. Besides, it can be seen from Fig. 9 and Fig. 10 that the 'AR-max' strategy has better radar performance when the

trade-off factor is within $[0.2, 0.6]$. Therefore, the proposed the 'AR-max' strategy can achieve a better performance trade-off between the radar system and the communication system.

VI. Conclusion

Considering the communication and radar detection performance trade-off, this paper proposed two waveform design strategies for the DFRC system based on MIMO and OFDM technologies in the frequency-selective multipath fading environment. ISI and achievable rate were employed as the performance metrics in the two proposed design strategies, respectively. In the CRB and ISI minimization based waveform design strategy, which can be viewed as an extension of the traditional single carrier based DFRC waveform to the frequency-selective multipath fading environment, we first solved the radar-strict problem and then allowed a tolerable deviation between the actual precoding design and the radar-strict design to achieve the performance trade-off between the radar system and the communication system. In the CRB minimization and achievable rate maximization based waveform design strategy, we proposed the WF-SQP algorithm to solve the optimization problem. Simulation results showed the superiority of the proposed waveform design strategies.

References

[1] Z. Chen, X. Y. Ma, B. Zhang, et al., "A survey on terahertz communications," *China Commun.*, vol. 16, no. 2, pp. 1-35, Feb. 2019.

[2] P. Zhang, X. Yang, J. Chen, et al., "A survey of testing for 5G: Solutions, opportunities, and challenges," *China Commun.*, vol. 16, no. 1, pp. 69-85, Jan. 2019.

[3] L. Wang, J. Mcgeehan, C. Williams, et al., "Application of cooperative sensing in radar-communications coexistence," *IET Commun.*, vol. 2, no. 6, pp. 856-868, Aug. 2008.

[4] B. Pual, A. R. Chiriyath and D. W. Bliss., "Survey of RF communications and sensing convergence research," *IEEE Access*, vol. 5, pp. 252-270, 2017.

[5] X. Shi, C. Yang, W. Xie, et al., "Anti-drone system with multiple surveillance technologies: Architecture, implementation, and challenges," *IEEE Commun. Mag.*, vol. 56, no. 4, pp. 68-74, Apr. 2018.

[6] I. Guvenc, F. Koohifar, S. Singh, et al., "Detection, tracking, and interdiction for amateur drones," *IEEE Commun. Mag.*, vol. 56, no. 4, pp. 75-81, Apr. 2018.

[7] H. Wymeersch, G. Seco-Granados, G. Destino, et al., "5G mmWave positioning for vehicular networks," *IEEE Wireless Commun.*, vol. 24, no. 6, pp. 80-86, Dec. 2017.

[8] P. Kumari, J. Choi, N. Gonzlez-Prelcic, et al., "IEEE 802.11ad-based radar: An approach to joint vehicular communication-radar system," *IEEE Trans. Veh. Technol.*, vol. 67, no. 4, pp. 3012-3027, Apr. 2018.

[9] Z. Feng, Z. Fang and Z. Wei, "Joint radar and communication: A survey," *China Commun.*, vol. 17, no. 1, pp. 1-27, Jan. 2020.

[10] A. R. Chiriyath, B. Paul and D. W. Bliss, "Radar-Communications Convergence: Coexistence, Cooperation, and Co-Design," *IEEE Trans. Cognit. Commun. Networking*, vol. 3, no. 1, pp. 1-12, Mar. 2017.

[11] Y. He, Y. Cai, G. Yu, et al., "Joint Transceiver Design for Dual-Functional Full-Duplex Relay Aided Radar-Communication Systems," *IEEE Trans. Commun.*, vol. 70, no. 12, pp. 8355–8369, Dec. 2022.

[12] F. Liu, C. Masouros, A. Li, et al., "MIMO radar and cellular coexistence: A power-efficient approach enabled by interference exploitation," *IEEE Trans. Signal Process.*, vol. 66, no. 14, pp. 3681-3695, Jul. 2018.

[13] A. Hassanien, M. Amin, Y. Zhang, et al. "Dual-function radar-communications: Information embedding using sidelobe control and waveform diversity," *IEEE Trans. Signal Process.*, vol. 64, no. 8, pp. 2168-2181, Apr. 2016.

[14] A. Hassanien, M. Amin, Y. Zhang, et al., "A dual function radar-communications system using sidelobe control and waveform diversity," *Proc. of IEEE Radar Conference*, Johannesburg, South Africa, Oct. 2015, pp. 1260-1263.

[15] A. Hassanien, E. Aboutanios, M. G. Amin, et al., "A dual-function MIMO radar-communication system via waveform permutation," *Digital Signal Process.*, vol. 83, pp. 118-128, Aug. 2018.

[16] H. Takahara, K. Ohno and M. Itami, "A study on UWB radar assisted by inter-vehicle communication for safety applications," *Proc. of the IEEE International Conference on Vehicular Electronics and Safety*, Istanbul, Turkey, Jul. 2012, pp. 99-104.

[17] L. Han, K. Wu, "Multifunctional Transceiver for Future Intelligent Transportation Systems," *IEEE Trans. Microwave Theory Tech.*, vol. 59, no. 7, pp. 1879-1892, Jul. 2011.

[18] L. Han, K. Wu, "24 Ghz integrated radio and radar system capable of time-agile wireless communication and sensing," *IEEE Trans. Microwave Theory Tech.*, vol. 60, no. 3, pp. 619-631, Mar. 2012.

[19] A. Mishra, M. Inggs, "FOPEN capabilities of commensal radars based on whitespace communication systems," *Proc. of the IEEE Conference on Electronics, Computing and Communication Technologies*, Bangalore, India, Jan. 2014, pp. 1-5.

[20] L. Reichardt, C. Sturm, F. Gr1nhaupt, et al., "Demonstrating the use of the IEEE 802.11P Car-to-Car communication standard for automotive radar," *2012 6th European Conference on Antennas and Propagation (EUCAP).*, pp. 1576-1580, 2012.

[21] H. Takase, M. Shinriki, "A dual-use radar and communication system with complete complementary codes," *Proc. of the 15th International Radar Symposium*, Gdansk, Poland, Jun. 2014, pp. 1-4.

[22] M. Jamil, H. Zepernick and M. I. Pettersson, "On integrated radar and communication systems using Oppermann sequences," *IEEE Military Communications Conference*, San Diego, CA, 2008, pp. 1-6.

[23] F. Liu, L. Zhou, C. Masouros, et al., "Toward dual-functional radar-communication systems: Optimal waveform design," *IEEE Trans. Signal Process.*, vol. 66, no. 16, pp. 4264-4279, Aug. 2018.

[24] J. Andrew Zhang, F. Liu, Christos Masouros, et al., "An overview of signal processing techniques for joint communication and radar sensing," available online at https://arxiv.org/abs/2102.12780.

[25] M. Roberton, E. R. Brown, "Integrated radar and communications based on chirped spread-spectrum techniques," *Proc. IEEE MTT-S Int. Microw. Symp. Dig.*, 2003, pp. 611–614.

[26] G. N. Saddik, R. S. Singh, and E. R. Brown, "Ultra-wideband multi-functional communications/radar system," *IEEE Trans. Microw. TheoryTechnol.*, vol. 55, no. 7, pp. 1431–1437, Jul. 2007.

[27] D. Ma, N. Shlezinger, T. Huang, et al., "Joint radar-communication strategies for autonomous vehicles: Combining two key automotive technologies," *IEEE Signal Process. Mag.*, vol. 37, no. 4, pp. 85–97, 2020.

[28] C. Sturm, W. Wiesbeck, "Waveform design and signal processing aspects for fusion of wireless communications and radar sensing," *Proc. IEEE*, vol. 99, no. 7, pp. 1236–1259, Jul. 2011.

[29] D. Gaglione, C. Clemente, C. V . Ilioudis, et al., "Fractional fourier based waveform for a joint radar communication system," *2016 IEEE Radar Conference*, 2016, pp. 1–6.

[30] F. Liu, C. Masouros, A. Li, et al., "MU-MIMO communications with MIMO radar: From co-existence to joint transmission," *IEEE Trans. Wireless Commun.*, vol. 17, no. 4, pp. 2755–2770, 2018.

[31] X. Liu, T. Huang, N. Shlezinger, et al., "Joint transmit beamforming for multiuser MIMO communications and MIMO radar," *IEEE Trans. Signal Process.*, vol. 68, pp. 3929–3944, 2020.

[32] X. Wang, Z. Fei, Z. Zheng, et al., "Joint waveform design and passive beamforming for RIS-assisted dualfunctional radar-communication system," *IEEE Trans. Veh. Technol.*, vol. 70, no. 5, pp. 5131–5136, 2021.

[33] F. Liu, Y. Liu, A. Li, et al., "Cramer-Rao Bound Optimization for Joint Radar-Communication Beamforming," *IEEE Trans. Signal Process.*, vol. 70, pp. 240-253, 2022.

[34] T. Zhang, Y. Zhao, D. Liu, et al., "Interference optimized dual-functional radar-communication waveform design with low PAPR and range sidelobe," *Signal Processing*, vol. 204, pp. 240-253, Mar. 2023.

[35] M. Jiang, G. Liao, Z. Yang, et al., "Integrated radar and communication waveform design based on a shared array," *Signal Processing*, vol. 182, May. 2021.

[36] H. Zhu, J. Wang, "Chunk-based resource allocation in OFDMA systems - Part I: chunk allocation," *IEEE Trans. Commun.*, vol. 57, no. 9, pp. 2734-2744, Sept. 2009.

[37] H. Zhu, J. Wang, "Chunk-based resource allocation in OFDMA systems - Part II: joint chunk, power and bit allocation," *IEEE Trans. Commun.*, vol. 60, no. 2, pp. 499-509, Dec. 2011.

[38] Z. Y. Xu, Athina Petropulu, "A Dual-Function Radar Communication System With OFDM Waveforms and Subcarrier Sharing," available online at https://arxiv.org/abs/2106.05878, Mar. 2022.

[39] T. Liu, L. Wu, Z. Zhang, et al., "Waveform Design for MIMO-OFDM Based Dual-functional Radar and Communication Systems," *14th International Conference on Wireless Communications and Signal Processing (WCSP 2022)*, Nanjing, China, Nov. 2022.

[40] X. Hu, C. Masouros and F. Liu, "MIMO-OFDM Dual-Functional Radar-Communication Systems: Low-PAPR Waveform Design," available online at https://arxiv.org/abs/2109.13148, Sep. 2021.

[41] S. Haykin. Communication systems, 4th edition. Beijing: Publishing House of Electronics Industry, Jan. 2020, pp. 597-599.

[42] I. Bekkerman, J. Tabrikian, "Target detection and localization using MIMO radars and sonars," *IEEE Trans. Signal Process.*, vol. 70, no. 10, pp. 3873-3883, Oct. 2006.

[43] Boyd, Stephen, and L. Vandenberghe, Convex optimization, Cambridge university Press, 2004.

[44] T.Viklands, "Algorithms for the weighted orthogonal procrustes problem and other least squares problems," *Ph.D. dissertation, Comput. Sci. Dept., Umea Univ.*, Umea, Sweden, 2006.

[45] C. G. Broyden, "The convergence of a class of double-rank minimization algorithms," *J. Inst. Math. Appl.*, vol. 6, no. 3, pp. 222-231, Sept. 1970.

[46] J. E. Dennis, J. J. More, "Quasi-Newton methods, motivation and theory," *SIAM Rev.*, vol. 19, no.1, pp. 46-89, 1977.

[47] G. Strang. Introduction to linear algebra, 5th edition. Wellesley: Wellesley-Cambridge Press, 2016.

[48] G. Ren, G. Y. Li, "Low-PAPR OFDM Using Sliding Window Tone Reservation With Low Complexity," *IEEE Trans. Commun.*, vol. 65, no. 11, pp. 5031-5042, Nov. 2017.

[49] I. Baig, V. Jeoti, "A new ZCT precoded OFDM system with pulse shaping: PAPR analysis," *IEEE Asia Pacific Conference on Circuits and Systems*, Kuala Lumpur, Malaysia, pp. 1131-1134, 2010.

[50] G. D. Pillo, Nonlinear Optimization, Lectures given at the C.I.M.E. Summer School held in Cetraro, Italy, Jul, 2007.